Inorganic Chemistry

Article

pubs.acs.org/IC

Group 14 Metal Terminal Phosphides: Correlating Structure with $|J_{MP}|$

Eric C. Y. Tam,[†] Nicola A. Maynard,[†] David C. Apperley,[‡] J. David Smith,[†] Martyn P. Coles,*[,†,§] and J. Robin Fulton*[,†,§]

[†]Department of Chemistry, University of Sussex, Falmer, Brighton, U.K.

[‡]Department of Chemistry, University of Durham, South Road, Durham, U.K.

Supporting Information

ABSTRACT: A series of heavier group 14 element, terminal phosphide complexes, M(BDI)(PR_2) (M = Ge, Sn, Pb; BDI = CH{(CH_3)CN-2,6-iPr$_2$C$_6$H$_3$}$_2$; R = Ph, Cy, $SiMe_3$) have been synthesized. Two different conformations (*endo* and *exo*) are observed in the solid-state; the complexes with an *endo* conformation have a planar coordination geometry at phosphorus (M = Ge, Sn; R = $SiMe_3$) whereas the complexes possessing an *exo* conformation have a pyramidal geometry at phosphorus. Solution-state NMR studies reveal through-space scalar coupling between the tin and the isopropyl groups on the *N*-aryl moiety of the BDI ligand, with *endo* and *exo* exhibiting different J_{SnC} values. The magnitudes of the tin−phosphorus and lead−phosphorus coupling constants, $|J_{SnP}|$ and $|J_{PbP}|$, differ significantly depending upon the hybridization of the phosphorus atom. For Sn(BDI)(P{$SiMe_3$}$_2$), $|J_{SnP}|$ is the largest reported in the literature, surpassing values attributed to compounds with tin−phosphorus multiple-bonds. Low temperature NMR studies of Pb(BDI)(P{$SiMe_3$}$_2$) show two species with vastly different $|J_{PbP}|$ values, interpreted as belonging to the *endo* and *exo* conformations, with sp^2- and sp^3-hybridized phosphorus, respectively.

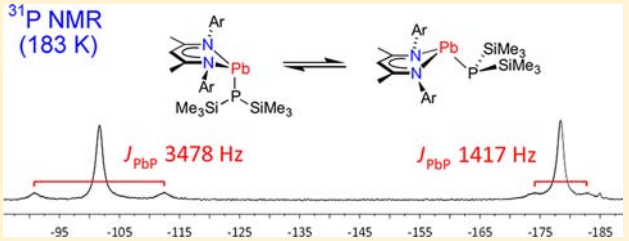

INTRODUCTION

M(BDI)X complexes of the heavier group 14 elements, (M = Ge, Sn, Pb; BDI = CH{$(CH_3)_2$CN-2,6-iPr$_2$C$_6$H$_3$}$_2$; X = monoanionic, terminal ligand) were initially synthesized over 10 years ago.[1] In the past 5 years, many studies have focused on the synthesis and structural characterization of new examples,[2] while others have explored the chemistry of the terminal ligands.[3] Although the geometry of the central atom, M, in these three-coordinate complexes is pyramidal, two different conformations are observed in the solid-state (Figure 1).[4] In

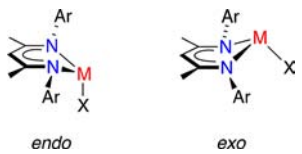

Figure 1. *Endo* and *exo* conformations of M(BDI)X (Ar = 2,6-iPr$_2$−C$_6$H$_3$).

the *endo* conformation, M and X are on the same side of the NCCCN plane of the BDI ligand with an approximately perpendicular M−X bond, and in the *exo* conformation M and X generally lie on opposite sides of the NCCCN plane, and the terminal ligand points away from the M(BDI) core. To a first approximation these conformations can be attributed to interactions of the terminal ligand, X, and the *N*-aryl groups of the BDI ligand. Smaller X-groups or those able to adopt a planar geometry can find room between the two *N*-aryl groups in an *endo* conformation whereas larger ligands force the molecule into the *exo* conformation to avoid steric conflict. Currently these observations are restricted to the solid-state and no spectroscopic markers differentiating these two conformations have been noted in solution.

Terminal phosphide complexes, M(BDI)(PR_2), have recently been reported. Roesky and Zhu have synthesized Ge(BDI)-(PPh_2),[5] which is *exo* in the solid-state with a pyramidal geometry at phosphorus. Driess has made the germanium[2d] and lead[2g] *bis*(trimethylsilyl) phosphide derivatives, M(BDI)(P-{$SiMe_3$}$_2$). Although crystal structure data for the latter two compounds show the germanium complex to be *endo* with a planar geometry at the phosphorus atom, and the lead homologue to be *exo* with a pyramidal phosphorus environment, no explanation for these differences has been presented. We show in this contribution that the shorter Ge−P bond (2.3912(8) Å) compared with Pb−P bond (2.715(2) Å) is not sufficient to account for this dichotomy.

To understand the preference for the group 14 phosphides to adopt either the *endo* or *exo* conformation, we have expanded this series of compounds. In particular we have targeted the previously unknown tin derivatives as intermediate between the germanium and the lead species, and taken advantage of additional spectroscopic information available from ^{119}Sn NMR experiments. Our spectroscopic studies have revealed previously unreported through-space scalar coupling between Sn and the isopropyl groups on the BDI *N*-aryl group, allowing us

Received: June 7, 2012
Published: August 17, 2012

   dx.doi.org/10.1021/ic301208d | *Inorg. Chem.* 2012, 51, 9403−9415

to look at the solution-phase conformations of these compounds. In addition, an exceptionally large coupling constant is observed in the tin *bis*(trimethylsilyl) phosphide derivative, prompting us to re-examine the lead homologue.

RESULTS AND DISCUSSION

Synthesis. The group 14 chlorides M(BDI)Cl, (**I** M = Ge,[1] **II** M = Sn,[1] **III** M = Pb[2e]) were synthesized according to literature procedures. Reaction of **I**–**III** with 1 equiv of $LiPR_2$ (R = Ph, Cy, $SiMe_3$) afforded the heteroleptic compounds $M(BDI)(PR_2)$ (**1** M = Ge, **2** M = Sn, **3** M = Pb; **a** R = Ph, **b** R = Cy, **c** R = $SiMe_3$) (Scheme 1). This strategy has previously

Scheme 1

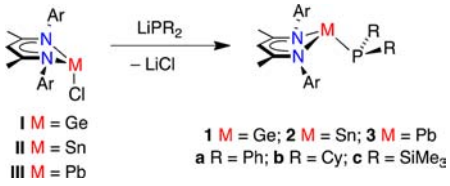

been used to synthesize $Ge(BDI)(PPh_2)$ **1a**[5] and $Ge(BDI)(P\{SiMe_3\}_2)$ **1c**;[2d] the lead analogue **3c** was made from the aryloxide $Pb(BDI)(OAr^\dagger)$ ($Ar^\dagger$ = 2,6-$tBu_2C_6H_3$).[2g] We found that **3c** may be synthesized in excellent yield (91%) by treatment of **III** with $LiP\{SiMe_3\}_2$. All compounds were isolated as solids that are stable at room temperature and could be handled under an inert atmosphere with no other precautions. In contrast solutions of **1**–**3**, in particular the lead derivatives, must be handled in the dark, as insoluble metallic precipitates were formed under ambient light conditions. Purification was achieved by crystallization, affording analytically pure products in good to excellent yields. In general, yields for the diphenylphosphides (**1a**, **2a**, and **3a**) were lower than those for other derivatives, and the compounds decomposed at lower temperatures. The frequent formation of tetraphenyldiphosphine, detected by $^{31}P\{^1H\}$ NMR (δ_P −14.8)[6] and crystal structure determination (see Supporting Information), suggests that the group 14 elements may mediate single-electron decomposition processes in the M–PPh_2 unit.

Crystallographic Analysis. Single crystal X-ray diffraction data have been obtained for all new phosphide compounds. Selected interatomic distances (Å) and angles (deg) are collected in Tables 1 (**1b**), 2 (**2a**, **2b**, **2c**), and 3 (**3a**, **3b**); these data are presented alongside those for **1a** and **1c** (Table 1) and **3c** (Table 3) for comparison. Crystal structure and refinement data are collected in Tables 6 (**1b**, **2a**, **2b**, **2c**) and 7 (**3a**, **3b**).

The germanium compound **1b** crystallizes as the monomeric, three-coordinate species, with a terminal–PCy_2 phosphide fragment (Figure 2). An *exo*-conformation is adopted in the solid-state, with the germanium 0.963(6) Å out of the plane defined by the NCCCN backbone of the BDI ligand. The coordination at germanium is pyramidal, with a degree of pyramidalization (DP),[7] of 80%. This latter measurement is a useful tool when comparing three-coordinate species; a DP of 100% is equivalent to a sum of angles of 270°, where as a DP of 0% is indicative of a planar geometry at the central atom (eq 1). The large DP at the germanium atom **1b** suggests that its lone-pair possesses marked s-character. The phosphorus atom also has a pyramidal coordination geometry (DP = 69%). The Ge–P bond length of 2.4724(8) Å is similar to that of **1a** (2.4746(11) Å),[5] but long compared with other terminal Ge(II)–PR_2 distances (R = aryl or alkyl; range 2.3938(13) to 2.4151(13) Å).[8] The Ge–P bonds in **1a** and **1b** are also longer

Table 1. Selected Bond Lengths (Å) and Angles (deg) for $Ge(BDI)(PCy_2)$ 1b Presented with Those for $Ge(BDI)(PPh_2)$ (1a)[5] and $Ge(BDI)(P\{SiMe_3\}_2)$ (1c)[2d] for Comparison

	1a[a]	1b	1c[a]
Ge–P	*2.4746(11)*	2.4724(8)	*2.3912(8)*
Ge–N1	*2.003(3)*	2.049(2)	*2.006(2)*
Ge–N2	*2.029(3)*	2.048(2)	*2.046(2)*
P–C30	*1.846(3)*	1.900(3)	
P–C36	*1.844(4)*	1.889(3)	
P–Si1			*2.219(1)*
P–Si2			*2.227(1)*
N1–Ge–N2	*88.20(11)*	88.05(8)	*90.20(9)*
N1–Ge–P	*99.24(8)*	102.52(6)	*103.46(7)*
N2–Ge–P	*99.29(8)*	101.35(7)	*94.93(6)*
C30–P–C36	*99.14(16)*	102.25(13)	
Ge–P–C30	*100.25(10)*	98.12(10)	
Ge–P–C36	*100.69(12)*	97.97(9)	
Si1–P–Si2			*110.13(5)*
Ge–P–Si1			*111.14(4)*
Ge–P–Si2			*133.93(4)*
DP(%) at Ge	*82*	*76*	*79*
DP(%) at P	*67*	*69*	*5*
θ^b	*+39.4(1)*	+39.9(1)	*−22.1*

[a]Different numbering scheme used; corresponding bond length/angle listed. [b]Fold angle between the planes defined by N1,C1,C2,C3,N2 atoms (plane 1) and N1,Ge,N2 atoms (plane 2). Positive values indicate exoconformer.

Table 2. Selected Bond Lengths (Å) and Angles (deg) for $Sn(BDI)(PPh_2)$ 2a, $Sn(BDI)(PCy_2)$ 2b, and $Sn(BDI)(P\{SiMe_3\}_2)$ 2c

	2a[a]	2b	2c
Sn–P	2.6612(12), 2.6417(12)	2.6309(7)	2.5526(7)
Sn–N(1)	2.211(3), 2.205(4)	2.233(2)	2.217(2)
Sn–N(2)	2.220(3), 2.224(4)	2.227(2)	2.2210(19)
P–C(30)	1.839(5), 1.844(5)	1.881(3)	
P–C(36)	1.836(5), 1.844(5)	1.892(3)	
P–Si(1)			2.2166(10)
P–Si(2)			2.2215(11)
N1–Sn–N2	83.76(13), 83.96(13)	83.23(8)	85.17(7)
N1–Sn–P	95.78(9), 96.11(10)	102.60(6)	101.77(5)
N2–Sn–P	104.53(10), 102.83(10)	99.95(6)	95.55(5)
C30–P–C36	102.5(2), 100.6(2)	103.30(12)	
Sn–P–C30	91.21(15), 94.49(14)	95.33(9)	
Sn–P–C36	102.07(15), 99.91(14)	96.18(8)	
Si1–P–Si2			111.32(4)
Sn–P–Si1			111.29(4)
Sn–P–Si2			136.45(4)
DP(%) Sn	84, 86	83	86
DP(%) P	71, 72	72	1
θ^b	+39.5(2), +39.8(2)	+39.0(1)	−20.9

[a]Two independent molecules in the unit cell; second value corresponds to equivalent bond in second molecule. [b]Fold angle between the planes defined by N1,C1,C2,C3,N2 atoms (plane 1) and N1,Sn,N2 atoms (plane 2). Positive values indicate *exo*-conformer.

dx.doi.org/10.1021/ic301208d | *Inorg. Chem.* 2012, 51, 9403–9415

Table 3. Selected Bond Lengths (Å) and Angles (deg) for Pb(BDI)(PPh_2) 3a and Pb(BDI)(PCy_2) 3b, Presented with Those for Pb(BDI)(P{$SiMe_3$}$_2$) (3c)[2g] for Comparison

	3a	3b	3c[a]
Pb−P	2.720(2)	2.6945(9)	*2.715(2)*
Pb−N(1)	2.324(6)	2.342(3)	*2.359(6)*
Pb−N(2)	2.347(6)	2.326(3)	*2.325(6)*
P−C(30)	1.845(8)	1.880(3)	
P−C(36)	1.818(9)	1.887(3)	
P−Si(1)			*2.260(3)*
P−Si(2)			*2.248(3)*
N1−Pb−N2	80.2(2)	80.79(9)	*81.2(2)*
N1−Pb−P	98.21(15)	102.03(7)	*97.32(15)*
N2−Pb−P	105.98(15)	99.25(7)	*103.18(16)*
C30−P−C36	101.3(4)	103.79(15)	
Pb−P−C30	87.3(2)	93.57(11)	
Pb−P−C36	101.1(3)	95.17(11)	
Si1−P−Si2			*99.45(11)*
Pb−P−Si1			*96.00(9)*
Pb−P−Si2			*110.25(10)*
DP(%) at Pb	84	87	*87*
DP(%) at P	78	75	*60*
θ[b]	+34.3(3)	+38.7(1)	*+43.9*

[a]Different numbering scheme used; corresponding bond length/angle listed. [b]Fold angle between the planes defined by N1,C1,C2,C3,N2 atoms (plane 1) and N1,Pb,N2 atoms (plane 2). Positive values indicate *exo*-conformer.

Table 4. Selected Spectroscopic Data for M(BDI)X (M = Ge, Sn, Pb; X = Cl, N{$SiMe_3$}$_2$, PPh_2, PCy_2, P{$SiMe_3$}$_2$) in C_6D_6[a]

		Cl	N{$SiMe_3$}$_2$	PPh_2	PCy_2	P{$SiMe_3$}$_2$
Ge	^{31}P			−36.0[b]	−14.1	−192.7[2d]
	^{29}Si					2.0[2d]
	$\lvert J_{PSi}\rvert$					17[2d]
Sn	^{31}P			−30.7	−15.4	−183.5
	^{29}Si		0.61/−4.7[25]			4.0
	^{119}Sn	−224[1]	−134[25]	125	358	39
	$\lvert J_{PSi}\rvert$					17
	$\lvert J_{SnP}\rvert$			978	964	2427
Pb	^{31}P			7.3	26.9	−116.6[2g]
	^{29}Si		−2.4/−3.1[2g]			7.4[2g]
	^{207}Pb	1413[26]	1824[2g]	3011	3981	−1737[2g]
	$\lvert J_{PSi}\rvert$					36[2g]
	$\lvert J_{PbP}\rvert$			1129	1084	2852[2g]

[a]Chemical shift/ppm; coupling constants/Hz. [b]Reference 5 reports the ^{31}P NMR chemical shift for Ge(BDI)(PPh_2) (**1a**) as δ −14.9 ppm.

than those in terminal silyl-substituted phosphides (2.291(4) to 2.426(7) Å),[2d,9] including **1c** (2.3912(8) Å).

$$\mathrm{DP}(\%) = [360 - \sum_{3}^{i=1} \alpha_i]/0.9 \quad (1)$$

In contrast to the *exo*-conformation in **1a**[5] and **1b**, Ge(BDI)(P{$SiMe_3$}$_2$) (**1c**) is *endo*.[2d] The germanium atom shows a similar degree of pyramidalization (DP = 79%) but it is 0.55 Å below the diketiminate plane (θ = −22.1°). In contrast with the three coordinate, Ge(II) terminal phosphide Ge(2,6-{trip}$_2$$C_6H_3$)(P{$SiMe_3$}$_2$) (trip = 2,4,6-*i*Pr$_3$$C_6H_2$),[9] which has a DP at phosphorus of 37%, and most tris(silyl-substituted) phosphines, where the DP ranges from 34 to 54%,[10] the phosphorus atom in **1c** has an almost planar geometry (DP = 5%). The only other structurally characterized example of a planar geometry at the phosphorus atom is that in P{Si(*i*Pr)$_3$}$_3$.[11] Although transition metal phosphide complexes can possess a phosphorus atom with a planar coordination geometry because of donation of the lone pair into an empty d orbital,[12] this is not the case with group 14 derivatives. Our observations suggest that the planarity of the geometry at phosphorus in **1c** derives from the steric influence of the BDI ligand rather than from electronic effects associated with the silyl-groups.

The molecular structures of tin compounds **2a**−**2c** (Figure 3) closely resemble those of their germanium analogues; each is monomeric with terminal phosphido groups. For compounds **2a** and **2b**, the tin atom is located 1.063(5)/1.067(6) Å and 1.067(3) Å above the NCCCN plane, respectively, corresponding to *exo*- conformations. In contrast, the conformation of **2c** is *endo*, with the tin 0.595(3) Å below the plane. The DP at tin (range 83 to 86%) does not vary significantly between conformations and does not depend on the phosphorus substituent.

The Sn−P distances in **2a** and **2b** (2.6612(12)/2.6417(12) Å and 2.6309(7) Å, respectively) are similar to those in other terminal Sn(II) phosphides with alkyl or aryl substituents, although examples are limited to the ate complex [Li(THF)-{Sn(P(*t*Bu)$_2$)(μ-P(*t*Bu)$_2$)$_2$}] (Sn−P = 2.684(4) Å),[13] and the amino-stabilized diphosphastannylenes, Sn[P(CH{$SiMe_3$}$_2$)-(C_6H_4-2-CH_2NMe_2)]$_2$,[14] and Sn[P(CH{$SiMe_3$}$_2$)(C_6H_4-2-NMe_2)]$_2$,[8b] (range Sn−P = 2.5995(10) to 2.6439(9) Å). The Sn−P bond in the silyl-derivative **2c** (2.5526(7) Å) is similar to those in other Sn(II) phosphides containing the -P{SiR_3}$_2$ group, that is, heterometallic Ba/Sn[15] and Ca/Sn[16] systems (Sn−P range 2.597(3)−2.615(2) Å), the diphosphanylstannylene, Sn(P{Si(*t*Bu)(trip)F}$_2$)$_2$ (Sn−P = 2.567(1) Å),[17] and Sn(2,6-{trip}$_2$$C_6H_3$)(P{$SiMe_3$}$_2$) (Sn−P = 2.527(1) Å).[9]

As in the germanium series, the geometry of the phosphorus atom is different in **2c** (DP = 1%), from that in both **2a** (DP = 71/72%) and **2b** (DP = 72%), and the compounds described above,[8b,13,14] (DP ranges from 25 to 47%) and is specific to the BDI-ligand system. The planar geometry is distorted, with the Sn−P−Si2 angle (136.45(4)°) significantly greater than the remaining angles (Figure 3b), presumably to relieve crowding by the aryl substituents.

As for **3c**,[2g] compounds **3a** and **3b** are monomers with terminal phosphido groups (Figure 4) and the pyramidally coordinated lead atoms (DP: **3a**, 84%; **3b**, 87%; **3c**, 87%) above the ligand plane (**3a**, 1.02(1) Å; **3b**, 1.127(4) Å; **3c**, 1.25 Å). The conformations are therefore *exo* for all members of the series, and in each case the geometry at phosphorus is pyramidal (DP: **3a**, 78%; **3b**, 75%; **3c**, 60%).

The Pb−P distances in **3a** (2.720(2) Å) and **3b** (2.6945(9) Å) are shorter than the terminal Pb−P bond lengths in [Li(THF){Pb(P(*t*Bu)$_2$)(μ-P(*t*Bu)$_2$)$_2$}] (Pb−P = 2.766(7) Å)[13] and [Pb(P(*t*Bu)$_2$)(μ-P(*t*Bu)$_2$)]$_2$ (Pb−P = 2.781(4) Å).[18] In contrast to the germanium and tin compounds, where the M−P distances for the silyl-substituted derivatives are about 3.5% shorter than the M−PR_2 distances, the Pb−P distance in **3c** (2.715(2) Å),[2g] is similar to the average of those in **3a** and **3b**.

Spectroscopic Analysis. In general, spectra obtained from solutions of *endo*- and *exo*- isomers of M(BDI)X show that the methyl groups within each *iso*-propyl group are inequivalent; that is, there are two apparent septets and four doublets in the

dx.doi.org/10.1021/ic301208d | Inorg. Chem. 2012, 51, 9403−9415

Table 5. Selected Spectroscopic Data for Previously Reported Compounds That Contain Tin−Phosphorus Multiple Bond Character, and Related Species[a]

compound	^{31}P	^{119}Sn	$\lvert J_{SnP}\rvert$	solvent
2c	−183.5	39	2427	C_6D_6
$R_2Sn{=}P(mes^*)$[27a]	204.7	658	2295	C_6D_6
$(Ar^{\ddagger})_2Sn{=}P(mes^*)$[27b]	170.7	500	2208	not reported
$(Ar)_2Sn(F){-}P(Li)(mes)\cdot W(CO)_5$[27c]	−121.0	35	2099	$CDCl_3$
$Li[(Ar^{\S})Sn{=}P(Ar^{\ddagger})]$[9]	229.7	*b*	2004	C_6D_6
$Sn(P\{Si^iPr_3\}\{Si(Ar^{\ddagger})_2F\})_2$[17]	−102.5	1551	1682	not reported
$Sn(P\{Si^iPr_3\}\{Si(Ar^{\ddagger})(^t Bu)F\})_2$[17]	−121.3	*b*	1628	not reported
$[Sn(\mu\text{-}P\{Ar^{\P}\})]_2$[27d]	255.6	967	1464	C_6D_6
$Sn(P\{SiPh_3\}_2)_2$[27e]	−175.4	*b*	1323	C_6D_6
$[Sn(P\{SiMe_3\}_2)(\mu\text{-}P\{SiMe_3\}_2)]_2$[27f]	−231.8[c]		1117[c] 1012[d]	C_6D_6
	−236.4[d]		1224[e] 1298[f]	
	−281.4[e] −295.3[f]			
$Sn(P\{Ph\}\{Ar^{\text{¥}}\})_2$[27g]	0.1	1101	891	C_6D_6

[a]Chemical shift/ppm; coupling constants/Hz; $Ar^{\ddagger}$ = 2,4,6-*i*$Pr_3C_6H_2$; $Ar^{\S}$ = 2,6-$(Ar^{\ddagger})_2C_6H_3$; $Ar^{\P}$ = 2,6-$(Ar)_2C_6H_3$; $Ar^{\text{¥}}$ = 2,6-$(mes)_2C_6H_3$. [b]^{119}Sn chemical shift not reported. [c]*trans*-terminal. [d]*cis*-terminal. [e]*cis*-bridging. [f]*trans*-bridging.

Table 6. Crystal Structure and Refinement Data for Ge(BDI)(PCy_2) 1b, Sn(BDI)(PPh_2) 2a, Sn(BDI)(PCy_2) 2b, and Sn(BDI)($P\{SiMe_3\}_2$) 2c

	1b	2a	2b	2c
formula	$C_{41}H_{63}GeN_2P$	$C_{41}H_{51}N_2PSn\cdot 0.5(C_7H_8)$	$C_{41}H_{63}N_2PSn$	$C_{35}H_{59}N_2PSi_2Sn$
formula weight	687.49	767.57	733.59	713.68
temperature (K)	173(2)	173(2)	173(2)	173(2)
wavelength (Å)	0.71073	0.71073	0.71073	0.71073
crystal size (mm)	0.21 × 0.09 × 0.06	0.16 × 0.10 × 0.08	0.17 × 0.11 × 0.07	0.18 × 0.10 × 0.06
crystal system	monoclinic	triclinic	monoclinic	monoclinic
space group	$P2_1/c$ (No.14)	$P\bar{1}$ (No.2)	$P2_1/c$ (No.14)	$P2_1/c$ (No.14)
a (Å)	10.0941(2)	12.6382(3)	9.9722(1)	12.1569(2)
b (Å)	23.5171(5)	17.6553(4)	23.7044(4)	15.7065(2)
c (Å)	17.2689(3)	19.5975(4)	17.4243(3)	23.4050(4)
α (deg)	90	69.422(1)	90	90
β (deg)	110.600(1)	84.810(1)	109.003(1)	119.547(1)
γ (deg)	90	74.862(1)	90	90
V (Å^3)	3837.24(13)	3951.75(15)	3894.37(10)	3887.82(10)
Z	4	4	4	4
D_c (Mg m^{-3})	1.19	1.29	1.25	1.22
absorption coefficient (mm^{-1})	0.87	0.72	0.73	0.78
θ range for data collection (deg)	3.47 to 26.73	3.40 to 27.09	3.44 to 27.11	3.48 to 27.10
reflections collected	48350	66909	57848	60531
independent reflections	8127 [R_{int} = 0.079]	17382 [R_{int} = 0.089]	8576 [R_{int} = 0.077]	8547 [R_{int} = 0.076]
reflections [$I > 2\sigma(I)$]	6180	11616	6730	6661
data/restraints/parameters	8127/0/408	17382/1/828	8576/0/408	8547/0/372
goodness-of-fit on F^2	0.990	1.030	1.023	0.991
final *R* indices [$I > 2\sigma$ (*I*)]	*R*1 = 0.046	*R*1 = 0.055	*R*1 = 0.037	*R*1 = 0.034
	*wR*2 = 0.108	*wR*2 = 0.123	*wR*2 = 0.072	*wR*2 = 0.070
R indices (all data)	*R*1 = 0.070	*R*1 = 0.099	*R*1 = 0.058	*R*1 = 0.056
	*wR*2 = 0.119	*wR*2 = 0.139	*wR*2 = 0.079	*wR*2 = 0.078
largest diff. peak/hole (e Å^{-3})	0.79 and −0.44	1.81 and −0.82	0.48 and −0.83	0.45 and −0.69

^{1}H NMR spectra. Correspondingly there are two resonances attributed to the $CHMe_2$ carbons and four assigned to the $CHMe_2$ carbons in the $^{13}C\{^1H\}$ NMR spectra. Analysis of the $^{13}C\{^1H\}$ NMR spectrum of chloride **II** revealed previously unreported coupling between *iso*-propyl-methine ($^4J_{SnC}$) and -methyl ($^5J_{SnC}$) resonances and tin, present as unresolved ^{117}Sn and ^{119}Sn satellites (Figure 5). Given the 4- and 5-bond separation between these atoms (for which through-bond coupling is likely to be weak) and the variation in J_{SnC} from resonance to resonance, we assign this to through-space scalar coupling (note: we have denoted the number of bonds between relevant nuclei as superscript *n*, i.e., ^nJ; however, this is used as a nomenclature tool and not an indication that the observed coupling is a through-bond phenomenon).[19] This through-space scalar coupling has previously been restricted to examples of coupling between NMR active nuclei, one of which is effectively 100% naturally abundant (i.e., ^{1}H, ^{19}F, ^{31}P); a recent observation of $\{^{19}F{-}^{117/119}Sn\}$ and $\{^{19}F{-}^{207}Pb\}$ coupling is most pertinent to this work.[20] Our results are the first to demonstrate that this phenomenon may be observed with

dx.doi.org/10.1021/ic301208d | *Inorg. Chem.* 2012, 51, 9403−9415

Table 7. Crystal Structure and Refinement Data for Pb(BDI)(PPh_2) 3a and Pb(BDI)(PCy_2) 3b

	3a	3b
formula	$C_{41}H_{51}N_2PPb$	$C_{41}H_{63}N_2PPb$
formula weight	810.01	822.09
temperature (K)	173(2)	173(2)
wavelength (Å)	0.71073	0.71073
crystal size (mm)	0.15 × 0.07 × 0.03	0.22 × 0.11 × 0.04
Crystal system	orthorhombic	monoclinic
space group	*I*2*cb* (No.45)	$P2_1/c$ (No.14)
a (Å)	15.9697(5)	9.9586(2)
b (Å)	18.3168(6)	23.7678(4)
c (Å)	25.8355(6)	17.4757(2)
β (deg)	90	108.531(1)
V (Å^3)	7557.2(4)	3921.93(11)
Z	8	4
D_c (Mg m^{-3})	1.42	1.39
absorption coefficient (mm^{-1})	4.54	4.37
θ range for data collection (deg)	3.43 to 27.09	3.43 to 27.09
reflections collected	24237	57828
independent reflections	8198 [R_{int} = 0.081]	8624 [R_{int} = 0.068]
reflections [$I > 2\sigma(I)$]	5814	6904
data/restraints/parameters	8198/1/408	8624/0/408
goodness-of-fit on F^2	0.986	1.031
final *R* indices [$I > 2\sigma(I)$]	*R*1 = 0.047	*R*1 = 0.029
	*wR*2 = 0.085	*wR*2 = 0.054
R indices (all data)	*R*1 = 0.086	*R*1 = 0.047
	*wR*2 = 0.096	*wR*2 = 0.058
largest diff. peak/hole (e Å^{-3})	0.68 and −1.40	0.99 and −0.97

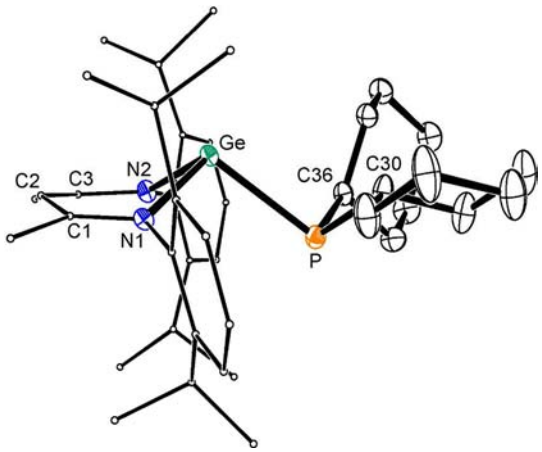

Figure 2. Molecular structure of Ge(BDI)(PCy_2) (**1b**) (H atoms omitted and BDI aryl groups C atoms minimized). Ellipsoid probability at 30%.

relatively insensitive but ubiquitous carbon-13 nuclei and to suggest that it may find general application for the study of species in solution.

Through-space scalar coupling implies that the nuclei come into close proximity in solution. The molecular structure of Sn(BDI)Cl is *endo*,[1] where for orthorhombic polymorph **II′** (see Supporting Information) the metal is displaced 0.801(3)/0.760(3) Å below the ligand plane (θ = −29.5(1)/−27.9(1)°). In the solid-state the range of Sn···C distances to the *iso*-propyl groups does not distinguish between those "adjacent" and "opposite" the chloride (Figure 5). For species with these precise conformations in solution, the coupling of the tin with

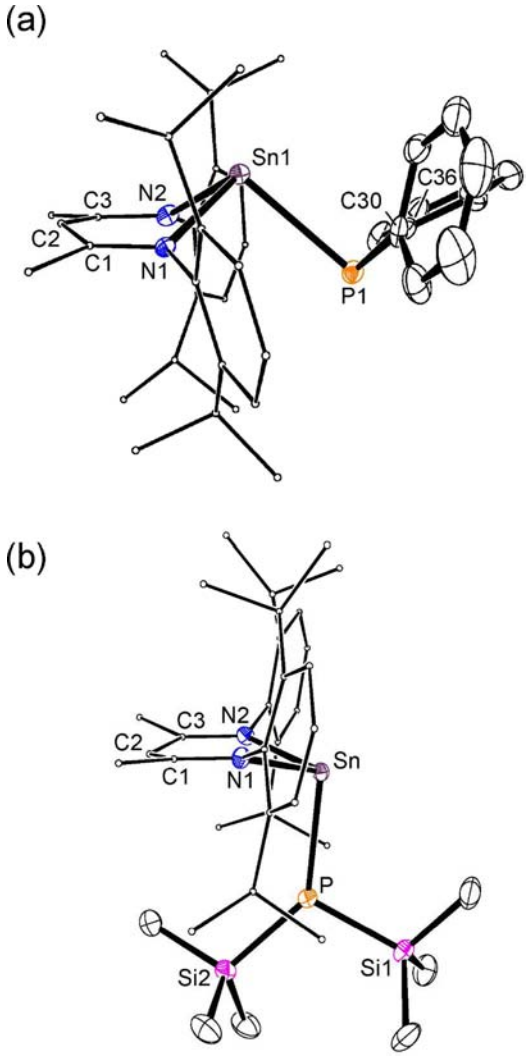

Figure 3. Molecular structure of (a) one of the independent molecules of Sn(BDI)(PPh_2) (**2a**) and (b) Sn(BDI)(P{$SiMe_3$}$_2$) (**2c**) (toluene solvate (**2a**) and H atoms omitted, and BDI aryl groups C atoms minimized). Ellipsoid probability 30%.

both *iso*-propyl groups should be similar. This is in contrast with the observed data where, within the resolution of the instrument, $^{4/5}J_{SnC}$ is only observed for one *iso*-propyl group (Figure 5a, a(b)$_2$). As such, although we are confident that the *endo* and *exo* conformations of M(BDI)X are maintained in solution (*vide infra*), their precise geometries are not static.

The NMR spectra for **1**−**3** conform to the same general pattern, consistent with a pyramidal coordination at the central atom in solution. The *iso*-propyl resonances in the ^{1}H and ^{13}C{^{1}H} NMR spectra show $^{6/7}J_{PH}$ and $^{5/6}J_{PC}$ coupling, respectively, which we also attribute to through-space scalar coupling between proximate nuclei. For example in **2a**, the low field septet in the ^{1}H NMR spectrum shows an additional coupling of 1.2 Hz (Supporting Information, Figure S7). The ^{31}P−^{1}H HMBC experiment shows correlation between phosphorus and this septet ($^6J_{PH}$) and between phosphorus and two CH*Me*$_2$ doublets ($^7J_{PH}$) (Supporting Information, Figure S8).

In the ^{13}C{^{1}H} NMR spectrum of **2a**, one of the methine- and one of the methyl-carbon resonances of the *iso*-propyl groups appears as a doublet with $^5J_{PC}$ of 6 Hz and $^6J_{PC}$ 8 Hz,

dx.doi.org/10.1021/ic301208d | *Inorg. Chem.* 2012, 51, 9403−9415

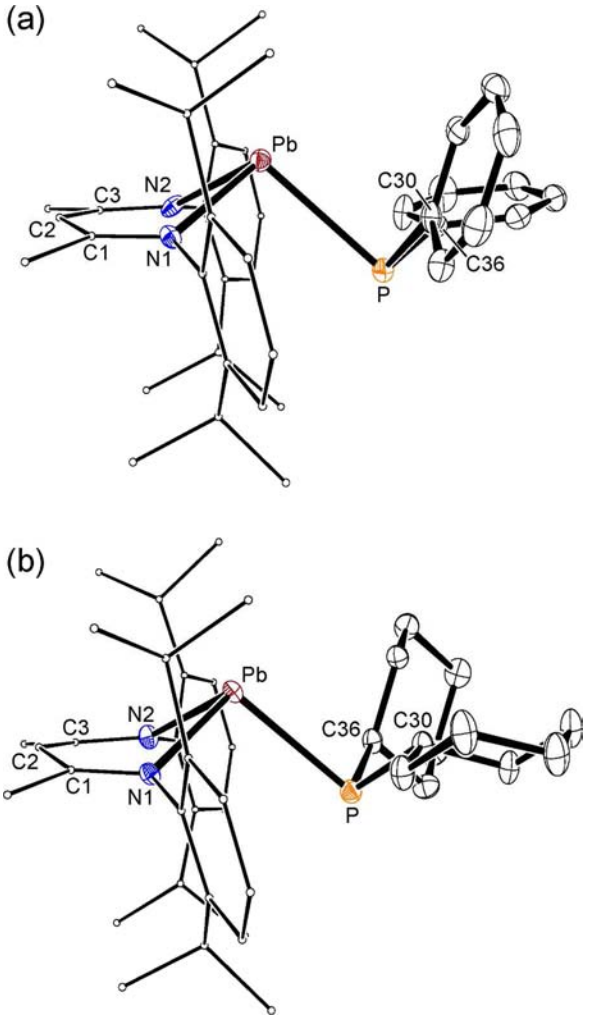

Figure 4. Molecular structures of (a) Pb(BDI)(PPh_2) (**3a**) and (b) Pb(BDI)(PCy_2) (**3b**) (H atoms omitted and BDI aryl groups C atoms minimized). Ellipsoid probability 30%.

respectively (Figure 6). There are also couplings to tin as described for **II** above. The coupling constants $^{4/5}J_{SnC}$ and $^{5/6}J_{PC}$ are observed from different resonances, suggesting that the tin and phosphorus atoms interact with different isopropyl groups. This correlates with the solid-state structure in which the opposite *iso*-propyl substituent is closest to the tin and the adjacent *iso*-propyl is closest to the phosphorus (Figure 6). The spectra of **2b** show similar couplings.

The tin atom in the *endo* isomer **2c** is approximately the same distance from the opposite and adjacent *iso*-propyl groups (Figure 7). However, only the adjacent substituents are close enough to interact with the phosphorus atom, suggesting that for both **II** and **2c**, it is the opposite *iso*-propyl groups that exhibit Sn···C coupling. For the methine resonance, there is an approximate difference of 15 Hz in $|^4J_{SnC}|$ between the *exo*- **2a** (36 Hz) and the *endo*- **2c** (21 Hz)/**II** (20 Hz). The tin amides Sn(BDI)(N^iPr_2) (*exo*) and Sn(BDI)(NHAr) (*endo*) show a similar difference with couplings of 35 and 19 Hz, respectively.[4] We feel confident, therefore, that the magnitude of this coupling may be used to determine whether an *exo*- or *endo*-conformation predominates in solution for compounds of general formula Sn(BDI)X.

The $^{13}C\{^1H\}$ NMR spectra of lead chloride Pb(BDI)Cl (**III**) and the phosphides **3a**, **3b**, and **3c** were examined to determine whether the corresponding through-space scalar coupling to ^{207}Pb nuclei was observable. Unfortunately, overlapping carbon resonances and the inherently lower receptivity of the lead atom relative to tin, prevented assignment of coupling in most cases. However, in *exo* compound Pb(BDI)(PPh_2) (**3a**), satellites due to $^{207}Pb\cdots^{13}C$ coupling between the "opposite" methine resonance and the lead was noted, with $^4J_{PbC}$ = 37 Hz (Supporting Information, Figure S9). Although $|J_{PbC}|$ for this interaction is similar to the values obtained for the *exo*- tin compounds, without further data we can not definitively say whether a similar trend in the magnitude of the through-space coupling is in operation for lead.

The ^{31}P NMR chemical shifts of **1**−**3** (Table 4) follow the expected pattern for a series of substituted compounds X-PR_2, with δ_P(X-PCy_2 **b**) > δ_P(X-PPh_2 **a**) ≫ δ_P(X-P{$SiMe_3$}$_2$ **c**). Recent studies of sterically crowded triarylphosphines show an upfield shift as the substituents become more bulky, for example, in $CDCl_3$: δ_P (ppm): PPh_3 −6; P(mes)$_3$ −36; P(Ar)$_3$ −50; P(trip)$_3$ −53 (mes = 2,4,6-$Me_3C_6H_2$, Ar = 2,6-iPr_2−C_6H_3), and the coordination at phosphorus becomes more planar (DP: PPh_3 57%;[21] P(mes)$_3$ 34%;[22] P(Ar)$_3$ 27%;[23] P(trip)$_3$ 28%[24]). Thus, a low frequency resonance is observed when the phosphorus is bound to silyl groups and as the atom adopts a more planar geometry.

The ^{119}Sn NMR chemical shifts for **2a**−**2c** appear at higher frequency than those from the chloride[1] and *bis*(trimethylsilyl)-amide[25] (Table 4), with **2b** > **2a** > **2c**. In contrast, while the ^{207}Pb chemical shifts for the diphenyl and dicyclohexyl compounds are at higher frequency than those of Pb(BDI)-chloride[26] and -*bis*(trimethylsilyl)amide,[2g] the *bis*(trimethylsilyl)phosphide **3c** is very strongly shielded and appears at δ_{Pb} −1737 ppm,[2g] corresponding to a $\Delta\delta_{Pb}$ of 5718 ppm compared with **3b**.

The $|^1J_{MP}|$ for **2** and **3** indicates that bonding within the M−P{$SiMe_3$}$_2$ group differs considerably from that in the alkyl and aryl substituted phosphides. Previous work concluded that the large $|^1J_{PbP}|$ in **3c** arose from a high 3s contribution from phosphorus in an intrinsically polarized Pb(δ^-)−P(δ^+) σ-bond.[2g] The couplings in **3a** (1129 Hz) and **3b** (1084 Hz) are considerably lower and similar to that reported for the terminal Pb−P(tBu)$_2$ group in the homoleptic dimer, [Pb(P(tBu)$_2$)(μ-P(tBu)$_2$)]$_2$ (1100 Hz).[18]

The coupling constant $|^1J_{SnP}|$ in **2c**, 2427 Hz, is exceptionally large (cf. **2a** 978 Hz, **2b** 964 Hz). The solid-state ^{31}P NMR spectrum (Supporting Information, Figure S10), with $|^1J_{SnP}|$ 2508 Hz, is in excellent agreement with the solution spectrum indicating the molecular species in solution and in the solid-state are similar. Previously large couplings have been considered indicative of compounds containing tin−phosphorus double bonds (Table 5).[9,17,27] For example, R_2Sn═P(mes*) (R = CH{$SiMe_3$}$_2$, mes* = 2,4,6-tBu$_3C_6H_2$) was reported as the first stable stannaphosphene (J_{SnP} 2295 Hz).[27a] As far as we are aware, however, there have been no examples of structurally characterized compounds having tin−phosphorus multiple bonds,[28] and therefore, given that the coupling constant in **2c** which contains a Sn−P single bond exceeds all those previous reported, we urge caution when parameter is cited as evidence for multiple bonding.

$|^1J_{PSi}|$ for **1c**[2d] and **2c** (both 17 Hz) from the $^{31}P\{^1H\}$ NMR spectra are toward the low end of the range observed for triorganosilylphosphines (7 to 50 Hz).[29] The small coupling constant (9.0 and 9.4 Hz for two diastereoisomers) observed in P(Si(iPr)$_3$)$_3$ was previously attributed to high ionic character in

dx.doi.org/10.1021/ic301208d | Inorg. Chem. 2012, 51, 9403−9415

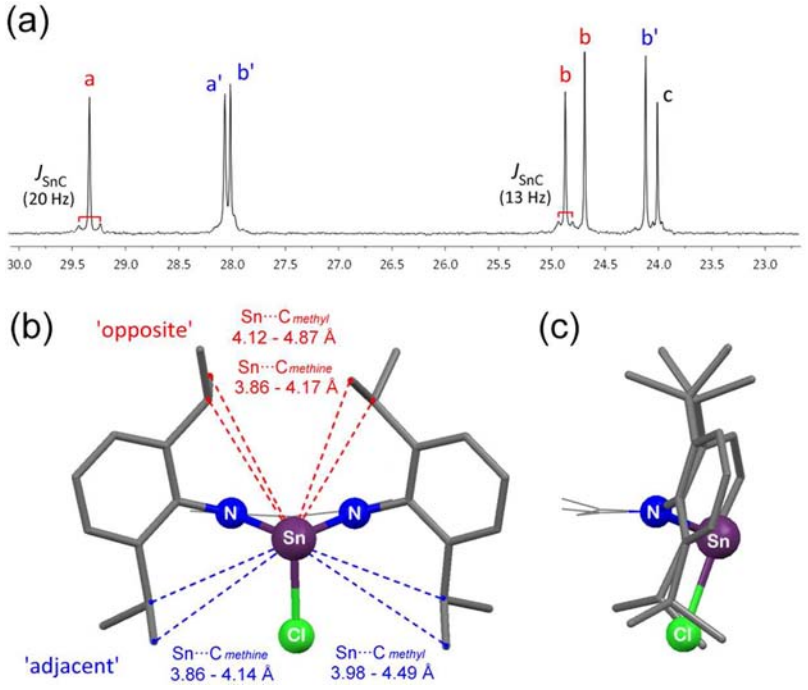

Figure 5. (a) $^{13}C\{^1H\}$ NMR spectra of Sn(BDI)Cl (**II**) in C_6D_6 showing J_{SnC}: **a** and **a′** CHMe$_2$, **b** and **b′** CHMe$_2$, **c** NCMe (where a(b)$_2$ and a′(b′)$_2$ indicate resonances from different pairs of iso-propyl groups); Schematic views of the relative position of the iso-propyl substituents with respect to the tin atom, with range of distances taken from crystal structure data, (b) facing the metallacycle; (c) side-view.

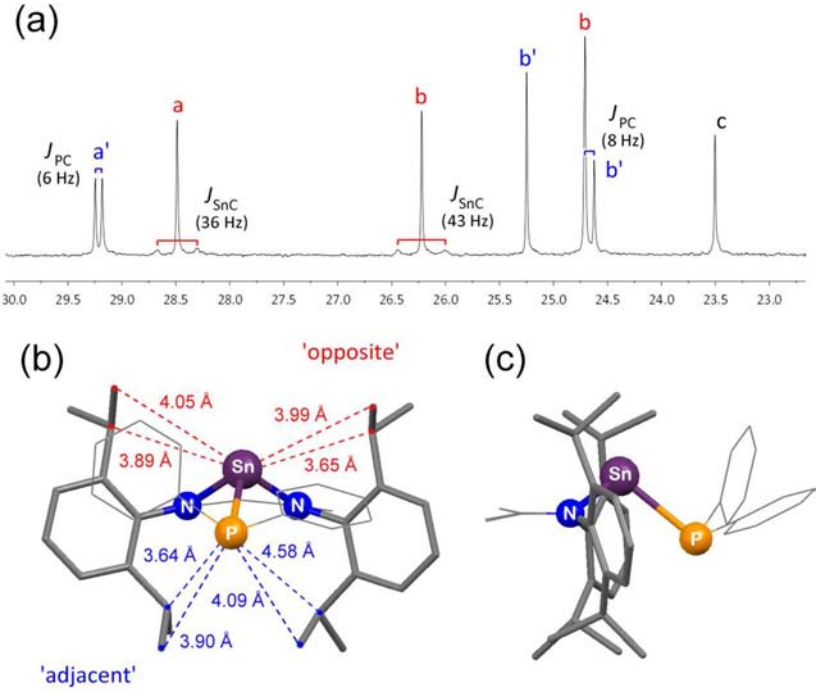

Figure 6. (a) $^{13}C\{^1H\}$ NMR spectra of Sn(BDI)(PPh$_2$) (**2a**) in C_6D_6 showing J_{SnC} and J_{PC}: **a** and **a′** CHMe$_2$, **b** and **b′** CHMe$_2$, **c** NCMe (where a(b)$_2$ and a′(b′)$_2$ indicate resonances from different pairs of iso-propyl groups); Schematic views of the relative position of the iso-propyl substituents with respect to the tin atom, taken from X-ray diffraction data: (b) facing the metallacycle; (c) side-view.

the Si−P bonds.[11] The coupling constant in the lead complex **3c** is 36 Hz.[2g]

As a first approximation, ^1J coupling constants involving phosphorus are dependent on the s-orbital contribution in the bonds and variations in the valence angle at phosphorus,[30] although account must also be taken of the ionicity within the bond and a possible change in the sign of J.[11] According to a simple valence bond description, one would therefore expect that compounds with an sp^3 phosphorus would show a lower $^1J_{MP}$ coupling than those with a sp^2 phosphorus atom with planar geometry. This fits the data for the tin compounds **2** if the solid-state structures are maintained in solution. However, the exceptionally large $|^1J_{PbP}|$ in **3c**, which is known to have a solid-state structure with a pyramidal geometry at the

dx.doi.org/10.1021/ic301208d | *Inorg. Chem.* 2012, 51, 9403−9415

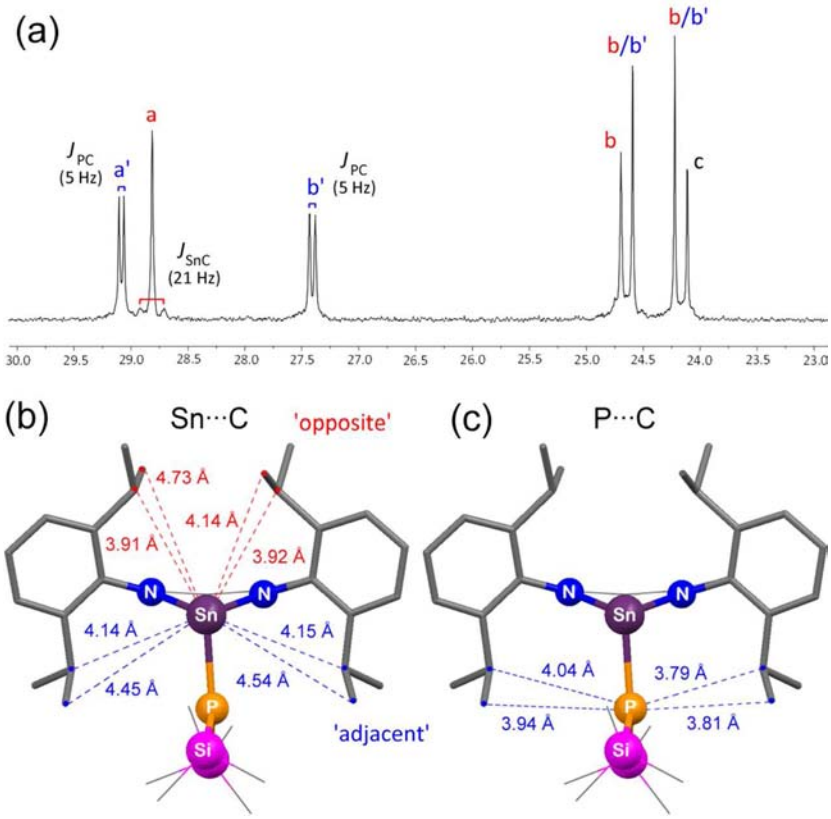

Figure 7. (a) $^{13}C\{^1H\}$ NMR spectra of Sn(BDI)(P{SiMe$_3$}$_2$) (**2c**) in C_6D_6 showing J_{SnC} and J_{PC}: **a** and **a′** CHMe$_2$, **b** and **b′** CHMe$_2$, **c** NCMe (where a(b)$_2$ and a′(b′)$_2$ indicate resonances from different pairs of iso-propyl groups); Schematic views of the relative position of the iso-propyl substituents with respect to the tin atom, taken from X-ray diffraction data:, (b) showing Sn···C distances; (c) showing P···C distances.

phosphorus atom, prompted us to examine the solution-state structures of the bis(trimethylsilyl) phosphido compounds in more detail.

The ^1H NMR spectra of **1c** and **2c**, recorded over the temperature range +30 to −80 °C, show that the Si*Me*$_3$ doublets observed at room temperature separate into two resonances of equal intensity as the temperature is lowered (**2c**, Supporting Information, Figure S11). The energy associated with this process is 11.2 kcal mol^{-1} (**1c**) and 10.5 kcal mol^{-1} (**2c**). The low temperature $^{31}P\{^1H\}$ spectra of each compound retain a single resonance, and in the case of tin, there is no significant increase in the $^1J_{SnP}$, suggesting that the M−P bond does not change significantly in this temperature range.

The separation of the Si*Me*$_3$ resonances in the ^1H NMR spectra at low temperature is reflected in silicon NMR experiments. At room temperature the $^{29}Si\{^1H\}$ NMR of **1c**[2d] and **2c** are doublets with $^1J_{PSi}$ = 17 Hz (Figure 8). As the temperature is lowered, two silicon resonances are observed, each of which shows coupling to phosphorus (not fully resolved for tin compound **2c**). These two silicon resonances reflect the different proton environments observed in the low temperature ^1H NMR spectra, confirmed through $^1H-^{29}Si$ HMBC experiments (Supporting Information, Figure S12). In each case there is a large disparity in the magnitude of the coupling to phosphorus, most evidently in the two low temperature resonances in **1c** where the difference in coupling constant (ΔJ_{Psi}) is 33 Hz (Figure 8). We propose that the large ΔJ_{PSi} is related to the variation in the bond angles about the planar coordination at phosphorus noted in the solid-state structures of **1c** and **2c** (Figure 3b). This is also supported by solid-state

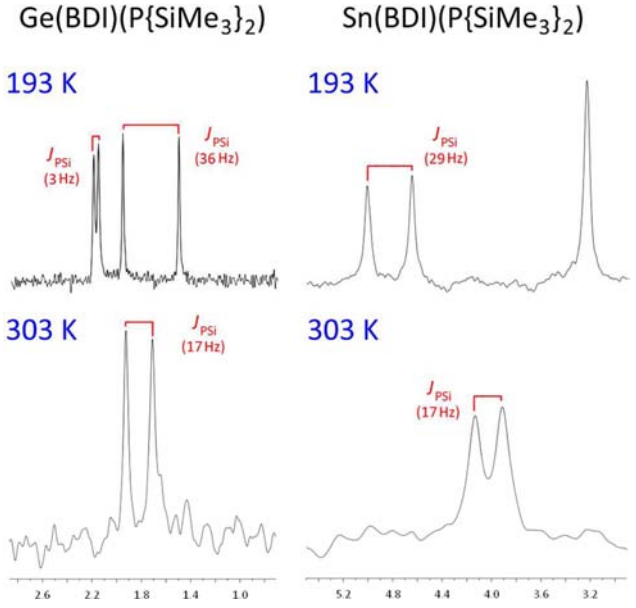

Figure 8. Solution-phase $^{29}Si\{^1H\}$ NMR spectra in toluene-d_8 for Ge(BDI)(P{SiMe$_3$}$_2$) (**1c**) and Sn(BDI)(P{SiMe$_3$}$_2$) (**2c**), recorded at 303 and 193 K.

$^{29}Si\{^1H\}$ NMR experiments (Figure 9a) that show two resonances for **2c**, with coupling resolved in one signal.

Variable temperature and solid-state NMR data have been obtained for Pb(BDI)(P{SiMe$_3$}$_2$). In contrast to the spectra of the tin compound, the solid-state $^{31}P\{^1H\}$ NMR spectrum of

dx.doi.org/10.1021/ic301208d | *Inorg. Chem.* 2012, 51, 9403−9415

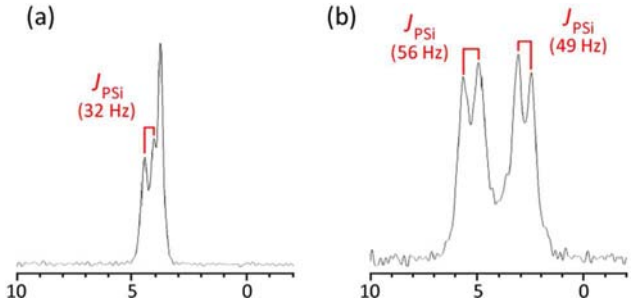

Figure 9. Solid-state $^{29}Si\{^1H\}$ NMR spectrum (a) Sn(BDI)(P{$SiMe_3$}$_2$) (**2c**); (b) Pb(BDI)(P{$SiMe_3$}$_2$) (**3c**) showing $^1J_{PSi}$ coupling.

3c differs from that acquired in solution. The chemical shift $\delta_{P(solid)}$ (ppm) is −173.5 (c.f. $\delta_{P(solution)}$ (ppm) −116.6), but the coupling is significantly lower ($^1J_{PbP(solid)}$ 1580 Hz), close to that predicted for phosphorus with a pyramidal geometry (vide supra). The solid-state ^{29}Si NMR spectrum (Figure 9b) shows two signals reflecting the different crystallographic environments for the two silicon atoms (torsion angle: Si1−P1−Pb1−N1 = −97.4°, Si2−P1−Pb1−N2 = 77.6°, Supporting Information, Figure S13). Each resonance shows a resolved one-bond coupling to phosphorus with similar $^1J_{PSi}$ (confirmed with decoupling experiments), indicating a similar magnetic environment for each $SiMe_3$ group consistent with the X-ray data.

Low temperature solution-state NMR spectra showed a broadening of the resonances for the Si*Me*$_3$ protons in the ^1H spectra although separation was not achieved at the low temperature limit. However, of major significance and in contrast to all other systems investigated, the $^{31}P\{^1H\}$ NMR spectra separated into two distinct resonances **A** and **B** at low temperature (Figure 10). The higher field resonance **B** is identified with that shown in the solid-state spectrum ($\delta_{P(solid)}$ (ppm): −173.5, J_{PbP} 1580 Hz; $\delta_{P(B)}$ (ppm): −178.5, J_{PbP} 1417 Hz) which we assign to the structure in which the coordination geometry at phosphorus is pyramidal. Resonance **A**, however, shows a much larger one-bond coupling between the lead and phosphorus bonds, as predicted for a planar sp^2-phosphorus coordination geometry ($\delta_{P(A)}$ (ppm): −101.7, J_{PbP} 3478 Hz).

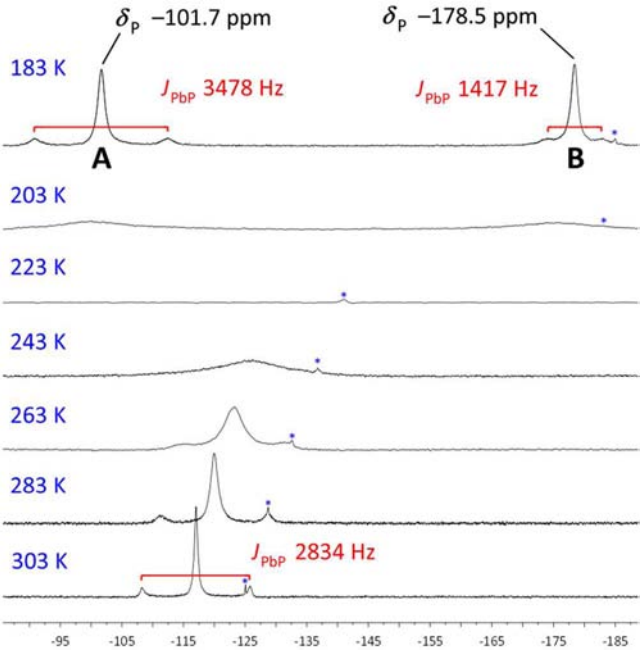

Figure 10. Variable temperature $^{31}P\{^1H\}$ NMR spectra in toluene-d_8 of Pb(BDI)(P{$SiMe_3$}$_2$) (**3c**) (* unidentified impurity).

These data lead us to conclude that the previously reported spectroscopic data for **3c** actually corresponds to an equilibrium mixture of two species (eq 2), one of which has a pyramidal

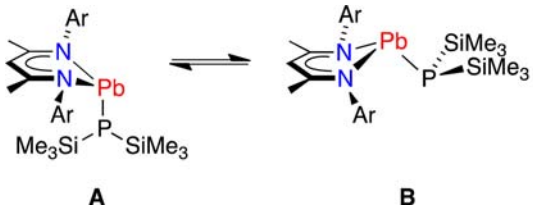

(2)

geometry at phosphorus (*exo* conformation, **B**) and the other having a planar geometry at phosphorus (*endo* conformation, **A**). It is important to note that in the tin and lead compounds **2c** and **3c** the one-bond coupling between the metal and phosphorus, for a planar coordination environment at phosphorus, vastly exceeds previously reported data.

CONCLUSIONS

The planar coordination at phosphorus in the bis-(trimethylsilyl) substituted phosphides **1c** and **2c** is unique to the BDI-system and has not been recorded previously in germanium and tin compounds. Terminal phosphides of heavier group 14 elements in sterically nonrestraining ligand systems have phosphorus atoms with pyramidal geometries, suggesting that this is most stable. It is tempting to assume that the different geometries noted in this study are a consequence of the shorter M−P bond lengths in the silyl-substituted phosphides (ave. **1a** and **1b** 2.4742(7) Å, **1c** 2.3912(8) Å; ave. **2a** and **2b** 2.6446(11) Å, **2c** 2.5526(7) Å). This contraction brings the phosphorus substituents into steric conflict with the *N*-aryl groups of the BDI ligand, forcing a planar arrangement to be more energetically favorable. This is a reasonable argument within the series of compounds containing a common central atom (Figure 11a). However, if considered in isolation, this parameter does not explain why compounds **1a**

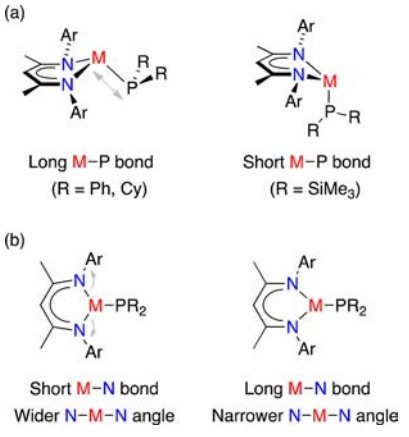

Figure 11. Factors that contribute to whether the phosphorus substituents are strongly influenced by proximity to the aryl groups of the BDI ligand (a) metal−phosphorus bond length; (b) bite angle of the ligand.

dx.doi.org/10.1021/ic301208d | *Inorg. Chem.* 2012, 51, 9403−9415

and **1b** have pyramidal coordination at phosphorus when the Ge−P bonds are shorter than the Sn−P bond in **2c**. One must also consider the reduced Ge−N bond lengths in **1a**, **1b**, and **1c** (ave. 2.061(2) Å, compared with those in the tin compounds ave. 2.220(3) Å). This causes the mouth of the ligand to be wider for germanium species (ave. N−Ge−N 88.80(8)°) than for tin (ave. N−Sn−N 84.03(1)°), reducing the influence of the aryl substituents in **1a** and **1b** (Figure 11b).

The Pb−N bond lengths in **3a**, **3b**, and **3c** are longer than those of the lighter homologues (ave. 2.337(5) Å) with a further reduction in N−M−N angle (ave. 80.7(2)°), in agreement with the arguments presented above. In this instance, however, there is no significant reduction in the Pb−P bond length for the *bis*(trimethysilyl) derivative so that, in the solid-state at least, the *exo* form predominates in all cases.

We have invoked through-space scalar coupling to explain the remarkable four to five bond coupling observed between Sn and C, five to six bond coupling observed between P and C as well as the six to seven bond coupling observed between P and H. Both $^{6/7}J_{PH}$ as well as $^{5/6}J_{PC}$ have been observed by others,[31] and through-space scalar coupling has been used to explain some of these long-range couplings.[31d] Our results are the first to report this phenomenon between relatively insensitive nuclei using standard one-dimensional ^{13}C and ^{119}Sn NMR spectroscopic techniques, although it is not unimaginable that this coupling has been previously overlooked. This scalar coupling is probably due to some as yet undetermined molecular orbital overlap between relevant nuclei. The analogous $^{4}J_{PbC}$ coupling was observed in **3a**, although we were unable to definitively observe coupling in **3b** and **3c**. This lack of coupling could partially be due to the smaller relative receptivity of ^{207}Pb nuclei relative to ^{119}Sn nuclei (2.01×10^{-3} and 4.53×10^{-3}, respectively, relative to the ^{1}H nuclei).[32]

The $|J_{SnP}|$ value for **2c** (2427 Hz) is the largest tin−phosphorus coupling reported to date, surpassing even those of compounds containing tin−phosphorus multiple bonds. The agreement between the solution- and solid-state NMR spectra confirm that this coupling comes from a Sn−P single bond, significantly widening the range of such $|J_{SnP}|$ values. A simple interpretation of this data is that the larger coupling in **2c** is due to the increased s-component to the Sn−P bond caused by a rehybridization of the phosphorus from sp^3 (pyramidal geometry) to sp^2 (planar geometry). This change in hybridization would result in greater s character in the bonding orbital on the phosphorus, thus further explaining the shorter Sn−P (and by analogy, Ge−P) bonds of the silyl substituted phosphide ligands. Computational studies to help understand these results are ongoing.

A similarly large coupling (2852 Hz) was previously noted for $|J_{PbP}|$ in **3c**, following the same general trend as that noted for the tin series. However, this result seems to be inconsistent with the pyramidal coordination at phosphorus observed in the crystal structure and the solid-state ^{31}P NMR data, for which a much lower value of $|J_{PbP}|$ was recorded (1580 Hz). Low temperature, solution-state ^{31}P NMR spectra of **3c** showed that the spectral data at 30 °C are an average of two signals **A** and **B**, which we assign to species in which the coordination at phosphorus is planar (**A**) and pyramidal (**B**). This once again increases the range of J values for Pb−P single bonds and the value previously reported as "unprecedentedly large" underestimates the upper limit by over 600 Hz.

We conclude that these J_{SnP} and J_{PbP} coupling data will be important in future work that investigates multiple bonding between these elements. While we have concentrated on the steric arguments in this contribution, possible underlying electronic effects are also under investigation, and we will report the results from these studies in due course.

EXPERIMENTAL SECTION

General Procedures. All manipulations were carried out under an inert atmosphere of dry nitrogen using standard Schlenk techniques or in an inert-atmosphere glovebox. Solvents were dried from the appropriate drying agent, distilled, degassed, and stored over 4 Å molecular sieves. ^{1}H and ^{13}C NMR spectra were recorded on Varian 400 and 500 MHz spectrometers. The solution-phase ^{29}Si, ^{31}P, ^{119}Sn and ^{207}Pb NMR spectra were recorded on a Varian 400 MHz spectrometer that was equipped with a X{^{1}H} broadband-observe probe. All spectra were recorded in C_6D_6 at 300 K, unless stated otherwise. The ^{1}H and ^{13}C NMR chemical shifts are given relative to residual solvent peaks, the ^{29}Si signals were externally referenced to $SiMe_4$, the ^{31}P signals were externally referenced to H_3PO_4(aq), the ^{119}Sn signals were externally referenced to $SnMe_4$, and the ^{207}Pb signals were externally referenced to $PbMe_4$. All assignments were confirmed by two-dimensional spectroscopy. Coupling constants J are quoted in hertz (Hz); coupling involving tin is quoted for the ^{119}Sn isotope. Solid-state NMR data were recorded on a Varian VNMRS spectrometer operating at 79.45 MHz (^{29}Si), 149.17 MHz (^{119}Sn), and 161.87 MHz (^{31}P). Spectral referencing is with respect to neat $SiMe_4$, 85% H_3PO_4 (by setting the signal from Brushite to 1 ppm) and $Sn(CH_3)_4$ (by setting the signal from $Sn(C_6H_{12})_4$ to −97.4 ppm). The samples were packed under nitrogen or helium; the spinning gas was nitrogen. The data for the X-ray structures were collected at 173 K on a Nonius Kappa CCD diffractometer [λ (Mo, Kα) 0.71073 Å] and refined using the SHELXL-97 software package.[33] Ge(BDI)Cl (**I**),[1] Sn(BDI)Cl (**II**),[1] Pb(BDI)Cl (**III**),[2e] Ge(BDI)(PPh_2) (**1a**),[5] and Ge(BDI)(P{$SiMe_3$}$_2$) (**1c**)[2d] were made according to published procedures.

Synthesis of LiPR$_2$. The required primary phosphine (HPR_2, R = Cy, Ph, $SiMe_3$) was added to an *n*-hexane solution under inert atmosphere. The solution mixture was cooled to −78 °C and an equimolecular amount of *n*-BuLi was added dropwise to the solution. The reaction was allowed to warm gradually to room temperature over a period of 20 h. Volatiles were evaporated under vacuum. The crude solid was washed with *n*-hexane and dried in vacuo. The purified solid was collected and stored at −35 °C under an inert atmosphere.

[CH{(CH$_3$)CN-2,6-*i*-Pr$_2$C$_6$H$_3$}$_2$GeP(C$_6$H$_{11}$)$_2$] (1b). Ge(BDI)Cl (0.311 g, 0.59 mmol) was dissolved in diethyl ether (∼ 15 mL) and added to $LiPCy_2$ (0.121 g, 0.59 mmol). The reaction mixture was stirred at room temperature for 40 h, after which the solution was filtered through a pad of Celite. The solvent was removed under vacuum, and the resulting crude purple solid was dissolved in a minimum amount of hexane, affording **1a** as purple crystals. Yield 0.375 g (92%). M.pt.: 199−200 °C (decomp.). Anal. Calcd. for $C_{41}H_{63}GeN_2P$ (*687.54*): C, 71.62; H, 9.24; N, 4.07. Found: C, 71.62; H, 9.21; N, 3.88. ^{1}H NMR: δ 7.17 (d, J = 7.6, 2H, Ar*H*), 7.11 (t, J = 7.6, 2H, Ar*H*), 7.04 (d, J = 7.6, 2H, Ar*H*), 4.74 (s, 1H, C*H*$_\gamma$), 4.08 (d sept, J = 6.8 and 2.4, 2H, C*H*Me$_2$), 3.44 (sept, J = 6.8, 2H, C*H*Me$_2$), 1.87 (*Cy**), 1.67 (d, J = 6.8, 6H, CH*Me*$_2$), 1.57 (*Cy**), 1.53 (s, 6H, NC*Me*), 1.37 (d, J = 6.8, 6H, CH*Me*$_2$), 1.30 (*Cy**), 1.20, 1.12 (d, J = 6.8, 6H, CH*Me*$_2$), 1.06−0.87 (*Cy**) 0.47 (br t, 2H, J_{HP} = 12.8 Hz, Cy-C*H*). * accurate integration of cyclohexyl proton resonances not possible because of overlap with other signals. ^{13}C{^{1}H} NMR: δ 167.2 (NCMe), 145.9, 144.5, 141.8 (*i*- and *o*-C_6H_3), 127.1, 125.1, 124.7 (*m*- and *p*-C_6H_3), 96.3 (γ-CH), 35.9 (br, Cy-CH_2), 35.2 (d, J_{PC} = 29, Cy-CH), 29.2 (d, J_{PC} = 9, $CHMe_2$), 28.9 (*C*HMe$_2$), 28.8 (d, J_{PC} = 7, Cy-CH_2), 26.8 (Cy-CH_2), 26.0, 25.3, 25.1 (CH*Me*$_2$), 24.6 (d, J_{PC} = 11, CH*Me*$_2$), 23.1 (NC*Me*). ^{31}P{^{1}H} NMR: δ −14.1. IR (Nujol, ν/cm^{-1}): 1556.6 (s), 1519.4 (s), 1319.5 (s), 1170.8 (s), 1019.0 (s), 793.7 (s). UV−vis (pentane), (λ_{max}, nm, (ε, M^{-1} cm^{-1})): 280.9 (17118), 352.0 (8874). EI-MS: m/z (%) 688 (18, M$^+$), 492 (100, [M-PCy_2]$^+$, 419 (10, [M-$GePCy_2$]$^+$).

dx.doi.org/10.1021/ic301208d | *Inorg. Chem.* 2012, 51, 9403−9415

[CH{(CH$_3$)CN-2,6-*i*-Pr$_2$C$_6$H$_3$}$_2$SnP(C$_6$H$_5$)$_2$] (2a). Compound **2a** was made according to the general procedure outlined for **1b** using Sn(BDI)Cl (0.300 g, 0.52 mmol) and LiPPh$_2$ (0.101 g, 0.52 mmol). The product was isolated as red-purple crystals from toluene. Yield 0.283 g (75%). M.pt.: 95−110 °C (decomp.). Anal. Calcd. for $C_{41}H_{51}N_2PSn$ (*721.54*): C, 68.25; H, 7.12; N, 3.88. Found: C, 68.06; H, 7.19; N, 3.95. ^{1}H NMR: δ 7.14 (dd, J = 7.6, 1.6, 2H, Ar*H*), 7.06 (t, J = 7.6, 2H, Ar*H*), 6.93 (dd, J = 7.6, 1.6, 2H, Ar*H*), 6.84−6.72 (m, 10H, P*Ph*$_2$), 4.71 (s, 1H, C*H*$_\gamma$), 4.08 (d sept, J = 6.8, 1.2, 2H, C*H*Me$_2$), 3.16 (sept, J = 6.8, 2H, C*H*Me$_2$), 1.67 (d, J = 6.8, 6H, CH*Me*$_2$), 1.52 (s, 6H, NC*Me*), 1.23, 1.12, 0.96 (d, 6H, J = 6.8, CH*Me*$_2$). ^{13}C{^{1}H} NMR: δ 167.6 (N*C*Me), 144.2, 143.5, 142.9 (*i*- and *o*-*C*$_6$H$_3$), 141.5 (d, J_{PC} = 32, *C*$_6$H$_5$), 135.1 (d, J_{PC} = 15, *C*$_6$H$_5$), 128.4 (d, J_{PC} = 6, *C*$_6$H$_5$), 127.0 (*o*-/*m* *C*$_6$H$_3$), 125.8 (*C*$_6$H$_5$), 125.2, 124.9 (*o*-/*m*-*C*$_6$H$_3$), 97.3 (*γ*-CH), 29.2 (d, J_{PC} = 6, *C*HMe$_2$), 28.5 (J_{SnC} = 36, *C*HMe$_2$), 26.2 (J_{SnC} = 43, CH*Me*$_2$), 25.3, 24.7 (CH*Me*$_2$), 24.7 (d, J_{PC} = 8, CH*Me*$_2$), 23.5 (NC*Me*). ^{31}P{^{1}H} NMR: δ −30.7 (J_{SnP} = 978). ^{119}Sn{^{1}H} NMR: δ 125 (d, J_{SnP} = 978). IR (Nujol, ν/cm^{-1}): 1578.2 (s), 1555.3 (s), 1515.8 (b), 1317.9 (s), 1265.7 (s), 1174.3 (s), 1099.4 (s), 1018.7 (s), 935.1 (s). UV−vis (pentane), (λ_{max}, nm, (ε, M^{-1} cm^{-1}): 283.9 (14960), 354.0 (13706).

[CH{(CH$_3$)CN-2,6-*i*-Pr$_2$C$_6$H$_3$}$_2$SnP(C$_6$H$_{11}$)$_2$] (2b). Compound **2b** was made according to the general procedure outlined for **1b** using Sn(BDI)Cl (0.380 g, 0.66 mmol) and a suspension of LiPCy$_2$ (0.135 g, 0.66 mmol) in toluene. The product was isolated as purple crystals from toluene at −30 °C. Yield 0.423 g (87%). M.pt.: 205−207 °C (decomp.). Anal. Calcd. for $C_{41}H_{63}N_2PSn$ (*733.64*): C, 67.12; H, 8.66; N, 3.82. Found: C, 67.03; H, 8.60; N, 3.75. ^{1}H NMR: δ 7.17 (dd, 2H, J = 7.7, 1.4, Ar*H*), 7.08 (t, 2H, J = 7.7, Ar*H*), 7.02 (dd, 2H, J = 7.7, 1.4, Ar*H*), 4.72 (s, 1H, C*H*$_\gamma$), 3.99 (d sept, 2H, J = 6.8, 1.6, C*H*Me$_2$), 3.32 (sept, 2H, J = 6.8, C*H*Me$_2$), 1.67 (d, 6H, J = 6.8, CH*Me*$_2$), 1.59 (s, 6H, NC*Me*), 1.54 (br, 6H, *Cy*‡), 1.31, 1.21, 1.15 (d, 6H, J = 6.8, CH*Me*$_2$), 1.00 (br, 8H, *Cy*‡). ‡ resonances for the remaining protons of the cyclohexyl substituents appear as an ill-defined broad feature spanning the region 0.6 and 2.1 ppm. ^{13}C{^{1}H} NMR: δ 167.9 (N*C*Me), 144.4, 144.1, 143.2 (*i*- and *o*-*C*$_6$H$_3$), 126.6, 124.9, 124.8 (*m*- and *p*-*C*$_6$H$_3$), 96.6 (*γ*-CH), 36.0 (br, Cy-CH$_2$), 32.8 (d, J_{PC} = 29, Cy-CH), 29.0 (d, J_{PC} = 7, *C*HMe$_2$), 28.5 (br, Cy-CH$_2$), 28.4 (CHMe$_2$), 26.6 (Cy-CH$_2$), 26.3, 25.3, 25.0 (CH*Me*$_2$), 24.8 (d, J_{PC} =10, CH*Me*$_2$), 23.6 (NC*Me*). ^{31}P{^{1}H} NMR: δ −15.4 (J_{SnP} = 953[§]) § coupling to ^{117}Sn and ^{119}Sn not resolved, therefore average coupling observed. ^{119}Sn{^{1}H} NMR: δ 358 (d, J_{SnP} = 964). IR (Nujol, ν/cm^{-1}): 1552.6 (s), 1517.6 (s), 1318.9 (s), 1173.8 (s), 1019.1 (s), 763.9 (s), 751.1 (s), 515.8 (s). UV−vis (pentane), λ_{max}, nm (ε, M^{-1} cm^{-1}): 284.0 (19409), 365.0 (10939).

[CH{(CH$_3$)CN-2,6-*i*-Pr$_2$C$_6$H$_3$}$_2$SnP{Si(CH$_3$)$_3$}$_2$] (2c). Compound **2c** was made according to the general procedure outlined for **1b** using Sn(BDI)Cl (0.436 g, 0.76 mmol) and a suspension of LiP{SiMe$_3$}$_2$ (0.140 g, 0.76 mmol) in toluene. The product was isolated as yellow crystals from pentane at −30 °C. Yield 0.503 g (93%). M.p.: 192−194 °C (decomp.). Anal. Calcd. for $C_{35}H_{59}N_2PSi_2Sn$ (*713.71*): C, 58.90; H, 8.33; N, 3.93. Found: C, 58.94; H, 8.28; N, 3.88. ^{1}H NMR: δ 7.22 (dd, J = 7.7, 1.6, 2H, Ar*H*), 7.16 (t, J = 7.6, 2H, Ar*H*), 7.09 (dd, J = 7.6, 1.6, 2H, *Ar*H), 4.95 (s, 1H, C*H*$_\gamma$), 3.97 (d sept, J = 6.8, 1.6, 2H, *C*HMe$_2$), 3.38 (sept, J = 6.8, 2H, *C*HMe$_2$), 1.61 (s, 6H, NC*Me*), 1.48, 1.32, 1.28, 1.12 (d, J = 6.8, 6H, CH*Me*$_2$), 0.46 (d, J_{SnH} = 124, J_{PH} = 4.4, J_{SiH} = 11.2, 18H, Si*Me*$_3$). ^{13}C{^{1}H} NMR: δ 167.1 (N*C*Me), 146.3, 143.6, 142.7 (*i*- and *o*-*C*$_6$H$_3$), 127.2, 125.5, 124.3 (*m*- and *p*-*C*$_6$H$_3$), 101.2 (*γ*-CH), 29.5 (d, J_{PC} = 5, *C*HMe$_2$), 29.3 (J_{SnC} = 21, *C*HMe$_2$), 27.8 (d, J_{PC} = 5, CH*Me*$_2$), 25.1, 25.0, 24.7 (CH*Me*$_2$), 24.5 (NC*Me*), 6.0 (d, J_{PC} = 10, J_{SnC} = 60, Si*Me*$_3$). ^{31}P{^{1}H} NMR: δ −183.5 (s, J_{PSi} = 17, J_{SnP} = 2427). ^{119}Sn{^{1}H} NMR: δ 39 (d, J_{SnP} = 2427). ^{29}Si{^{1}H} NMR: δ 4.0 (d, J_{PSi} = 17). IR (Nujol, ν/cm^{-1}): 1551.4 (s), 1521.0 (s), 1314.4 (s), 1239.1 (s), 1167.6 (s), 1020.4 (s), 935.2 (s), 831.3 (b), 794.8 (s), 757.2 (s), 628.1 (s). UV−vis (pentane), λ_{max}, nm (ε, M^{-1} cm^{-1}): 231.0 (34501), 373.1 (13015). MS *m*/*z* (EI): 713, 537, 403, 202, 160, 73, 46.

[CH{(CH$_3$)CN-2,6-*i*-Pr$_2$C$_6$H$_3$}$_2$PbP(C$_6$H$_5$)$_2$] (3a). Compound **3a** was made according to the general procedure outlined for **1b** using Pb(BDI)Cl (0.250 g, 0.38 mmol) and LiPPh$_2$ (0.073 g, 0.38 mmol). The product was isolated as red crystals from hexane. Yield 0.189 g, (61%). M.pt.: 265−266 °C (decomp.). Anal. Calcd. for $C_{41}H_{51}N_2PPb$ (*810.03*): C, 60.79; H, 6.35; N, 3.46. Found: C, 60.92; H, 6.51; N, 3.38. ^{1}H NMR: δ 7.21 (d, J = 7.6, 2H, Ar*H*), 7.05 (t, J = 7.6, 2H, Ar*H*), 6.96 (d, J = 7.6, 2H, Ar*H*), 6.86 (t, J = 7.3, 4H, C$_6$*H*$_5$), 6.75 (t, J = 7.3, 2H, C$_6$*H*$_5$), 6.53 (t, J = 7.3, 4H, C$_6$*H*$_5$), 4.59 (s, 1H, C*H*$_\gamma$), 4.04 (sept, J = 6.8, 2H, C*H*Me$_2$), 3.06 (sept, J = 6.8, 2H, C*H*Me$_2$), 1.69 (d, J = 6.8, 6H, CH*Me*$_2$), 1.64 (s, 6H, NC*Me*), 1.29, 1.13, 0.86 (d, 6H, J = 6.8, CH*Me*$_2$). ^{13}C{^{1}H} NMR: δ 166.0 (NCMe), 144.6, 143.6, 143.1 (*i*- and *o*-*C*$_6$H$_3$), 142.3 (d, J_{PC} = 38, *C*$_6$H$_5$), 135.7 (d, J_{PC} = 16, *C*$_6$H$_5$), *, 126.5 (*o*-/*m* *C*$_6$H$_3$), 126.4 (*C*$_6$H$_5$), 124.8, 124.6 (*o*-/*m*-*C*$_6$H$_3$), 98.6 (*γ*-CH), 29.0 (d, J_{PC} = 5, *C*HMe$_2$), 28.0 (J_{PbC} = 37, *C*HMe$_2$), 26.5 (CH*Me*$_2$), 25.1 (d, J_{PC} = 9, CH*Me*$_2$), 25.1, 24.7 (CH*Me*$_2$), 23.9 (NC*Me*) * remaining C$_6$H$_5$ resonance obscured by solvent. ^{31}P{^{1}H} NMR: δ 7.3 (J_{PbP} = 1129). ^{207}Pb{^{1}H} NMR: 3011 (d, J_{PbP} = 1129). IR (Nujol, ν/cm^{-1}): 1551.7 (s), 1512.8 (s), 1317.4 (s), 1172.7 (s), 1017.6 (s), 933.5 (s), 793.2 (s). UV−vis (pentane), (λ_{max}, nm, (ε, M^{-1} cm^{-1}): 259.1 (18623), 312.0 (17694).

[CH{(CH$_3$)CN-2,6-*i*-Pr$_2$C$_6$H$_3$}$_2$PbP(C$_6$H$_{11}$)$_2$] (3b). Compound **3b** was made according to the general procedure outlined for **1b** using Pb(BDI)Cl (0.500 g, 0.79 mmol) and a suspension of LiPCy$_2$ (0.155 g, 0.79 mmol) in toluene. The product was isolated as deep red crystals from toluene and −30 °C. Yield 0.59 g (95%). M.pt.: 154−155 °C (decomp.). Anal. Calcd. for $C_{41}H_{63}N_2PPb$ (*822.13*): C, 59.90; H, 7.72; N, 3.41. Found: C, 60.01; H, 7.59; N, 3.29. ^{1}H NMR: δ 7.21 (dd, J = 7.4, 1.6, 2H, Ar*H*), 7.05 (t, J = 7.4, 2H, Ar*H*), 7.02 (dd, J = 7.4, 1.6, 2H, Ar*H*), 4.61 (s, 1H, C*H*$_\gamma$), 3.95 (d sept, J = 6.8, 0.8, 2H, C*H*Me$_2$), 3.25 (sept, J = 6.8, 2H, C*H*Me$_2$), 1.73 (s, 6H, NC*Me*), 1.69 (d, J = 6.8, 6H, CH*Me*$_2$), 1.63 (br, 6H, Cy-C*H* and *Cy*‡), 1.25, 1.24, 1.18 (d, 6H, J = 6.8, CH*Me*$_2$), 1.01 (br, 8H, *Cy*‡) ‡ resonances for the remaining protons of the cyclohexyl substituents appear as an ill-defined broad feature spanning the region 0.5 and 1.9 ppm. ^{13}C{^{1}H} NMR: δ 166.5 (NCMe), 144.8, 144.0, 143.1 (*i*- and *o*-*C*$_6$H$_3$), 126.0, 124.6, 124.3 (*m*- and *p*-*C*$_6$H$_3$), 97.8 (*γ*-CH), 39.0 (br, Cy-CH$_2$), 34.0 (d, J_{PC} = 34, Cy-CH), 28.8 (d, J_{PC} = 5, CHMe$_2$), 28.7 (br, Cy-CH$_2$), 27.9 (CHMe$_2$), 26.6 (CH*Me*$_2$), 26.5 (Cy-CH$_2$), 25.5 (d, J_{PC} =10, CH*Me*$_2$), 25.1, 25.0 (CH*Me*$_2$), 23.8 (NC*Me*). ^{31}P{^{1}H} NMR: δ 26.9 (J_{PbP} = 1084). ^{207}Pb{^{1}H} NMR: δ 3981 (d, J_{PbP} = 1084). IR (Nujol, ν/cm^{-1}): 1555.7 (s), 1514.57 (s), 1318.71 (s), 1172.0 (s), 934.7 (s), 788.5 (s). UV−vis (pentane), (λ_{max}, nm, (ε, M^{-1} cm^{-1}): 280.9 (17118), 352.0 (8874).

[CH{(CH$_3$)CN-2,6-*i*-Pr$_2$C$_6$H$_3$}$_2$PbP{Si(CH$_3$)$_3$}$_2$], (3c). Pb(BDI)Cl (0.24 g, 0.369 mmol) was dissolved in toluene (20 mL) and added directly to LiP(TMS)$_2$ (0.07 g, 0.369 mmol). The reaction mixture was stirred at room temperature for 4 h. The red solution was filtered through a pad of Celite. The volatiles were evaporated under vacuum, and the solid was dissolved *n*-hexane for recrystallization at −35 °C (0.27 g, 91%). ^{1}H NMR (499.91 MHz, C$_6$D$_6$, 303 K): δ 7.22 (dd, J = 7.5, 2.0, 2H, *m*-H), 7.12 (t, J = 7.5, 2H, *p*-H), 7.09 (dd, J = 7.5, 2.0, 2H, *m*-H), 4.75 (s, 1H, *γ*-C*H*), 3.92 (d sept, J = 7.0, 1.0, 2H, C*H*Me$_2$), 3.29 (sept, J = 6.5, 2H, C*H*Me$_2$), 1.64 (s, 6H, NC*Me*), 1.52 (d, J = 6.5, 6H, CH*Me*$_2$), 1.31 (d, J = 7.0, 6H, CH*Me*$_2$), 1.26 (d, J = 6.5, 6H, CH*Me*$_2$), 1.16 (d, J = 7.0, 6H, CH*Me*$_2$), 0.30 (d, J = 4.0, 18H, Si*Me*$_3$). ^{13}C{^{1}H} NMR (100.46 MHz, C$_6$D$_6$, 303 K): δ 166.2 (NCMe), 145.5 (*ipso*-C), 144.7 (*o*-C), 143.6 (*o*-C), 127.0 (*m*-H), 125.6 (*m*-H), 124.4 (*p*-H), 103.0 (*γ*-CH), 29.0 (CHMe$_2$), 28.4 (d, J_{PC} = 6.3, CH*Me*$_2$), 28.2 (d, J_{PC} = 5.0, CHMe$_2$), 26.1 (CH*Me*$_2$), 25.1 (CH*Me*$_2$), 25.1 (CH*Me*$_2$), 25.0 (NC*Me*), 7.5 (d, J_{SiC} = 9.8, Si*Me*$_3$). ^{31}P{^{1}H} NMR (161.72 MHz, C$_6$D$_6$, 303 K): δ −116.6 (J_{PbP} = 2874). ^{29}Si{^{1}H} NMR (79.37 MHz, C$_6$D$_6$, 303 K): δ 7.2 (d, J_{PSi} = 36). UV−vis (pentane) λ_{max}, nm (ε, M^{-1} cm^{-1}): 382.0 (7900).

■ ASSOCIATED CONTENT

Ⓢ Supporting Information

Thermal ellipsoid plots of **1b**, **2a**−**2c**, **3a**−**3b**; selected solution- and solid-state NMR data; crystal structure data for polymorphic Sn(BDI)Cl (**II′**) and Ph$_2$P-PPh$_2$. This material is available free of charge via the Internet at http://pubs.acs.org.

dx.doi.org/10.1021/ic301208d | *Inorg. Chem.* 2012, 51, 9403−9415

AUTHOR INFORMATION

Corresponding Author

*Fax: +64 (0)4 463 5237. Phone: +64 (0)4 463 9799. E-mail: martyn.coles@vuw.ac.nz (M.P.C.); j.robin.fulton@vuw.ac.nz (J.R.F.).

Present Address

[§]School of Chemical and Physical Sciences, P.O. Box 600, Victoria University of Wellington, Wellington, New Zealand.

Author Contributions

The manuscript was written through contributions of all authors. All authors have given approval to the final version of the manuscript.

Notes

The authors declare no competing financial interest.

ACKNOWLEDGMENTS

We wish to thank Dr. Ian Crossley for the kind donation of $HP\{SiMe_3\}_2$ and Dr. Iain Day for helpful and stimuating discussion during the preparation of this manuscript. We acknowledge Dr. Lorrenzo Ferro for X-ray data of Sn(BDI)Cl (**II′**) and Lisa Harris for the X-ray data of Ph_2P-PPh_2. We thank the University of Sussex for financial support.

REFERENCES

(1) Ding, Y.; Roesky, H. W.; Noltemeyer, M.; Schmidt, H.-G.; Power, P. P. *Organometallics* **2001**, *20*, 1190−1194.

(2) (a) Taylor, M. J.; Saunders, A. J.; Coles, M. P.; Fulton, J. R. *Organometallics* **2011**, *30*, 1334−1339. (b) Jana, A.; Sarish, S. P.; Roesky, H. W.; Schulzke, C.; Samuel, P. P. *Chem. Commun.* **2010**, *46*, 707−709. (c) Jana, A.; Nekoueishahraki, B.; Roesky, H. W.; Schulzke, C. *Organometallics* **2009**, *28*, 3763−3766. (d) Yao, S.; Brym, M.; Merz, K.; Driess, M. *Organometallics* **2008**, *27*, 3601−3607. (e) Chen, M.; Fulton, J. R.; Hitchcock, P. B.; Johnstone, N. C.; Lappert, M. F.; Protchenko, A. V. *Dalton Trans.* **2007**, 2770−2778. (f) Fulton, J. R.; Hitchcock, P. B.; Johnstone, N. C.; Tam, E. C. Y. *Dalton Trans.* **2007**, 3360−3362. (g) Yao, S.; Block, S.; Brym, M.; Driess, M. *Chem. Commun.* **2007**, 3844−3846. (h) Pineda, L. W.; Jancik, V.; Starke, K.; Oswald, R. B.; Roesky, H. W. *Angew. Chem., Int. Ed.* **2006**, *45*, 2602−2605.

(3) (a) Ferro, L.; Hitchcock, P. B.; Coles, M. P.; Fulton, J. R. *Inorg. Chem.* **2012**, *51*, 1544−1551. (b) Ferro, L.; Hitchcock, P. B.; Coles, M. P.; Cox, H.; Fulton, J. R. *Inorg. Chem.* **2011**, *50*, 1879−1888. (c) Jana, A.; Objartel, I.; Roesky, H. W.; Stalke, D. *Dalton Trans.* **2010**, *39*, 4647−4650. (d) Jana, A.; Roesky, H. W.; Schulzke, C. *Dalton Trans.* **2010**, *39*, 132−138. (e) Jana, A.; Tavcar, G.; Roesky, H. W.; John, M. *Dalton Trans.* **2010**, *39*, 9487−9489. (f) Jana, A.; Roesky, H. W.; Schulzke, C.; Samuel, P. P. *Organometallics* **2010**, *29*, 4837−4841. (g) Tam, E. C. Y.; Johnstone, N. C.; Ferro, L.; Hitchcock, P. B.; Fulton, J. R. *Inorg. Chem.* **2009**, *48*, 8971−8976. (h) Jana, A.; Roesky, H. W.; Schulzke, C. *Inorg. Chem.* **2009**, *48*, 9543−9548. (i) Jana, A.; Objartel, I.; Roesky, H. W.; Stalke, D. *Inorg. Chem.* **2009**, *48*, 7645−7649. (j) Jana, A.; Objartel, I.; Roesky, H. W.; Stalke, D. *Inorg. Chem.* **2009**, *48*, 798−800. (k) Dove, A. P.; Gibson, V. C.; Marshall, E. L.; Rzepa, H. S.; White, A. J. P.; Williams, D. J. *J. Am. Chem. Soc.* **2006**, *128*, 9834−9843.

(4) Harris, L. A.-M.; Coles, M. P.; Fulton, J. R. *Inorg. Chim. Acta* **2011**, *369*, 97−102.

(5) Yang, Y.; Zhao, N.; Zhu, H.; Roesky, H. W. *Inorg. Chem.* **2012**, 2425−2431.

(6) Appel, R.; Milker, R. *Chem. Ber.* **1975**, *108*, 1783−1790.

(7) Maksić, Z. B.; Kovačević, B. *J. Chem. Soc., Perkin Trans. 2* **1999**, 2623−2629.

(8) (a) Izod, K.; Stewart, J.; Clark, E. R.; Clegg, W.; Harrington, R. W. *Inorg. Chem.* **2010**, *49*, 4698−4707. (b) Izod, K.; Stewart, J.; Clegg, W.; Harrington, R. W. *Organometallics* **2010**, *29*, 108−116. (c) Izod, K.; McFarlane, W.; Allen, B.; Clegg, W.; Harrington, R. W. *Organometallics* **2005**, *24*, 2157−2167. (d) Druckenbrodt, C.; du Mont, W.-W.; Ruthe, F.; Jones, P. G. *Z. Anorg. Allg. Chem.* **1998**, *624*, 590−594.

(9) Johnson, B. P.; Almstätter, S.; Dielmann, F.; Bodensteiner, M.; Scheer, M. *Z. Anorg. Allg. Chem.* **2010**, *636*, 1275−1285.

(10) (a) Dzambasky, A.; Baumgartner, J.; Hassler, K. *J. Organomet. Chem.* **2009**, *694*, 757−762. (b) Cappello, V.; Baumgartner, J.; Dransfield, A.; Hassler, K. *Eur. J. Inorg. Chem.* **2006**, 4589−4599. (c) Nieger, M.; Niecke, E.; Dany, S. *Z. Kristallogr.−New Cryst. Struct.* **1997**, *212*, 249−250. (d) Westerhausen, M.; Lang, G.; Schwarz, W. *Chem. Ber.* **1996**, *129*, 1035−1040. (e) Bruckmann, J.; Krüger, C. *Acta Crystallogr.* **1995**, *C51*, 1152−1155. (f) Petrie, M. A.; Power, P. P. *J. Chem. Soc., Dalton Trans.* **1993**, 1737−1745.

(11) Driess, M.; Merz, K.; Monsé, C. *Z. Anorg. Allg. Chem.* **2000**, *626*, 2264−2268.

(12) Weber, L.; Meine, G.; Boese, R.; Augart, N. *Organometallics* **1987**, *6*, 2484−2488.

(13) Arif, A. M.; Cowley, A. H.; Jones, R. A.; Power, J. M. *J. Chem. Soc., Chem. Commun.* **1986**, 1446−1447.

(14) Izod, K.; Stewart, J.; Clark, E. R.; McFarlane, W.; Allen, B.; Clegg, W.; Harrington, R. W. *Organometallics* **2009**, *28*, 3327−3337.

(15) Westerhausen, M.; Hausen, H.-D.; Schwarz, W. *Z. Anorg. Allg. Chem.* **1995**, *621*, 877−888.

(16) Westerhausen, M.; Enzelberger, M. M.; Schwarz, W. *J. Organomet. Chem.* **1995**, *491*, 83−90.

(17) Driess, M.; Janoschek, R.; Pritzkow, H.; Rell, S.; Winkler, U. *Angew. Chem., Int. Ed. Engl.* **1995**, *34*, 1614−1616.

(18) Cowley, A. H.; Giolando, D. M.; Jones, R. A.; Nunn, C. M.; Power, J. M. *Polyhedron* **1988**, *7*, 1909−1910.

(19) Mallory, F. B. *J. Am. Chem. Soc.* **1973**, *95*, 7747−7752.

(20) Wei, Z.; Yang, J.-H.; Vreshch, V. D.; Zabula, A. V.; Filatov, A. S.; Dikarev, E. V. *Inorg. Chem.* **2011**, *50*, 7295−7300.

(21) Daly, J. J. *J. Chem. Soc.* **1964**, 3799−3810.

(22) Blount, J. F.; Maryanoff, C. A.; Mislow, K. *Tetrahedron Lett.* **1975**, *16*, 913−916.

(23) Boeré, R. T.; Bond, A. M.; Cronin, S.; Duffy, N. W.; Hazendonk, P.; Masuda, J. D.; Pollard, K.; Roemmele, T. L.; Tran, P.; Zhang, Y. *New J. Chem.* **2008**, *32*, 214−231.

(24) Sasaki, S.; Sutoh, K.; Murakami, F.; Yoshifuji, M. *J. Am. Chem. Soc.* **2002**, *124*, 14830−14831.

(25) Jana, A.; Roesky, H. W.; Schulzke, C.; Döring, A.; Beck, T.; Pal, A.; Herbst-Irmer, R. *Inorg. Chem.* **2009**, *48*, 193−197.

(26) Jana, A.; Sarish, S. P.; Roesky, H. W.; Schulzke, C.; Döring, A.; John, M. *Organometallics* **2009**, *28*, 2563−2567.

(27) (a) Couret, C.; Escudie, J.; Satge, J.; Raharinirina, A.; Andriamizaka, J. D. *J. Am. Chem. Soc.* **1985**, *107*, 8280−8281. (b) Ranaivonjatovo, H.; Escudie, J.; Couret, C.; Satge, J. *J. Chem. Soc., Chem. Commun.* **1992**, 1047−1048. (c) Rodi, A. K.; Ranaivonjatovo, H.; Escudie, J.; Kerbal, A. *Phosphorus, Sulfur Silicon Relat. Elem.* **1997**, *126*, 157−169. (d) Merrill, W. A.; Wright, R. J.; Stanciu, C. S.; Olmstead, M. M.; Fettinger, J. C.; Power, P. P. *Inorg. Chem.* **2010**, *49*, 7097−7105. (e) Matchett, M. A.; Chiang, M. Y.; Buhro, W. E. *Inorg. Chem.* **1994**, *33*, 1109−1114. (f) Goel, S. C.; Chiang, M. Y.; Rauscher, D. J.; Buhro, W. E. *J. Am. Chem. Soc.* **1993**, *115*, 160−169. (g) Rivard, E.; Sutton, A. D.; Fettinger, J. C.; Power, P. P. *Inorg. Chim. Acta* **2007**, *360*, 1278−1286.

(28) Fischer, R. C.; Power, P. P. *Chem. Rev.* **2010**, *110*, 3877−3923.

(29) Verkade, J. G.; Mosbo, Z. A. *^{31}P NMR Spectroscopy in Stereochemical Analysis*; VCH: Weinheim, Germany, 1987.

(30) Pople, J. A.; Santry, D. P. *Mol. Phys.* **1964**, *8*, 1−18.

(31) (a) Gholivand, K.; Ghadimi, S.; Naderimanesh, H.; Forouzanfar, A. *Magn. Reson. Chem.* **2001**, *39*, 684−688. (b) Griffin, C. E.; Gordon, M. *J. Am. Chem. Soc.* **1967**, *89*, 4427−4431. (c) Malon, M.; Koshino, H. *Magn. Reson. Chem.* **2007**, *45*, 770−776. (d) Hierso, J.-C.; Armspach, D.; Matt, D. *C. R. Chim.* **2009**, *12*, 1002−1013.

(32) Harris, R. K.; Becker, E. D.; de Menezes, S. M. C.; Goodfellow, R.; Granger, P.; Int, C. *Magn. Reson. Chem.* **2002**, *40*, 489−505.

(33) Sheldrick, G. M. *SHELXL-97, Program for the Refinement of Crystal Structures*; University of Göttingen: Göttingen, Germany, 1997.